# Double-resonance study of predissociation of the $j\ ^3\Delta_g$ state of $H_2$

L. J. Lembo and D. L. Huestis
*Molecular Physics Department, SRI International, Menlo Park, California 94025*

S. R. Keiding and N. Bjerre
*Institute of Physics, University of Aarhus, 8000 Aarhus C, Denmark*

H. Helm
*Molecular Physics Department, SRI International, Menlo Park, California 94025*

(Received 18 March 1988)

A photoionization-photodissociation double-resonance technique has been employed to excite transitions from selected rovibrational levels of the metastable $c\ ^3\Pi_u^-$ state to the rapidly predissociated $j\ ^3\Delta_g$ state of $H_2$. The photodissociation resonances arise from the configuration interaction between the $j\ ^3\Delta_g$ and $i\ ^3\Pi_g$ states, and exhibit the asymmetry of Fano-Beutler profiles. These resonances have widths that decrease with increasing $v'$ from 29 to 10 $cm^{-1}$; calculated predissociation widths show the same vibrational trend but are consistently 30% smaller. Results have been obtained for the rovibrational energy spacings of high-$v$ levels within each state, and are in good agreement with theory. Photon energies for the $c$-to-$j$ state transitions are slightly larger than those predicted theoretically.

## I. INTRODUCTION

Despite its apparent simplicity, a great deal of interest and uncertainty still remain concerning the structure and spectrum of the hydrogen molecule. This is especially true for the high vibrational levels of the excited electronic states. The triplet manifold in particular has recently become the subject for numerous experimental investigations.[1–9] The ability to study the triplet system of $H_2$ hinges upon the existence of the metastable $2p\pi\ c\ ^3\Pi_u^-$ state[10] (see Fig. 1). For spectroscopic studies the $c$-state molecules are commonly formed by electron-impact excitation[2,3,5,9] of a thermal hydrogen beam or by charge transfer of a fast $H_2^+$ beam at keV energies.[4,6–8]

Spectroscopic investigations employing the fast-beam technique have used primarily two means of monitoring photoabsorption from the $c\ ^3\Pi_u^-$ state. These are (1) detection of neutral atomic fragments[4] resulting from direct photodissociation, predissociation, and bound free photon emission; and (2) detection of $H_2^+$ ions,[6] resulting from direct photoionization and from autoionization. Using either detection scheme a rich spectrum is obtained, due in part to the broad rotational and vibrational distributions of the parent $H_2^+$ ions used to form the metastable hydrogen beam. Strong coupling between continuum and bound states results in large linewidths for many of the transitions. Consequently, transitions from neighboring lower-state levels often overlap in the wavelength spectrum, making the contribution of individual levels difficult to resolve.

An example of this spectral overlap problem appears in excitation of the $3d\delta\ j\ ^3\Delta_g$ state. Levels of this state lying above the potential barrier of the $3d\pi\ i\ ^3\Pi_g$ state ($v > 5$) are rapidly predissociated by the continuum of the $i\ ^3\Pi_g$ state (see Fig. 1). The spectral overlap is partially resolved in experiments which measure the kinetic energy of the dissociation fragments as a function of excitation wavelength.[7,11] Such studies have very clearly demonstrated the modification of the $i$-state continuum by the presence of the rapidly predissociated $j$-state levels. The technique has, however, not yet been employed to isolate

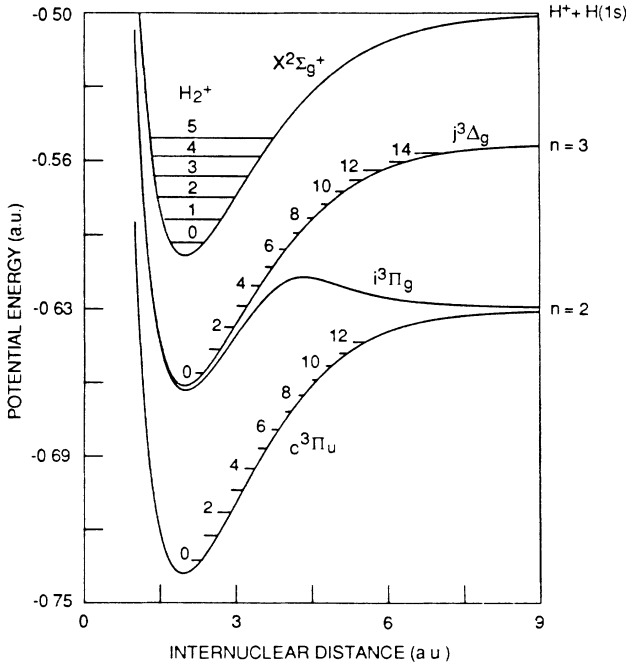


FIG. 1. Pertinent potential curves of $H_2$ and $H_2^+$.

 

excitation profiles of individual $j$-state levels.

In the present study, we introduce a double-resonance technique that monitors all photoabsorptions from selected $c\ ^3\Pi_u^-$ $(v'',N'')$ levels by detecting a reduction in the ionization rate on a transition to an autoionizing level. We report the application of this method to the study of photodissociation transitions to high vibrational levels of the $j\ ^3\Delta_g$ state lying above the potential barrier of the $i\ ^3\Pi_g$ state. This technique provides straightforward rovibrational assignments of both the upper and lower levels of the transitions and allows the identification of weak and broad transitions that would otherwise remain unresolved. The double-resonance dissociation spectra allow one to resolve the weakly asymmetric Fano-Beutler photodissociation line shapes.

## II. EXPERIMENTAL ARRANGEMENT

The experiments described below were performed on two similar fast-neutral-beam spectrometers, one at SRI and one at the University of Aarhus. Detailed descriptions of the fast-neutral-beam apparatus used in these studies have appeared elsewhere.[6,12] A beam of $H_2^+$ ions, extracted from an electron-impact or hot-filament discharge ion source, is accelerated to an energy of 1–2 keV and mass-selected. The $H_2^+$ ions are directed into a cesium-vapor cell, where near-resonant charge transfer populates the metastable $c$ state and results in typical neutral-beam currents of 50 pA. This beam is then coaxially excited in an ultra-high vacuum region, using the double-resonance scheme to be described below. Ions created as a result of the laser excitation are either deflected directly into a channel-electron multiplier, or energy analyzed before being detected. Ion counts are registered with gated scalers interfaced to a PDP11 microcomputer via a CAMAC dataway.

Figure 2 depicts the optical arrangement for double-resonance probing of the neutral beam. One laser (henceforth designated laser I) was a broadband (1 $cm^{-1}$) tunable cw dye laser operating at a power of 100–500 mW over the wavelength range investigated in these studies. Laser I is tuned to acquire the photoionization spectrum of the $c$ state. Figure 3 shows a typical ionization spectrum of the $H_2$ $c\ ^3\Pi_u^-$ state, obtained by monitoring the resulting photoions. As discussed in more detail in a separate paper,[13] these ionization resonances are single-photon transitions from high vibrational levels of the $c$ state to autoionizing resonances lying above the first ionization limit of $H_2$. For the double-resonance experiments, a narrow-band cw ring laser (laser II) operating between 200 and 500 mW was tuned to a fixed frequency, corresponding to one of the ionization resonances in Fig. 3, in order to label a particular rovibrational level of the $c$ state. While monitoring the ionization signal produced by laser II, the broadband laser (laser I) was frequency scanned over the wavelength range 5400 to 6400 Å.

The two laser beams are chopped at different frequencies, combined with a polarizing beamsplitter, and then steered into the fast-beam chamber. Ion counts are recorded by two counters (henceforth designated counters 1 and 2), each gated with a digital-delay generator to detect ions for the two different excitation conditions necessary for the acquisition of double-resonance spectra; this gating scheme is shown in Fig. 4. Each gating cycle consists of four 4.5 msec intervals, each separated by a dead time of $\sim 1$ msec, during which the mechanical chopper is blocking or unblocking the continuous-wave lasers. Counter 1 is gated to record ions which are created while either laser I or II is on separately. Counter 2 records ions which are created from neutral molecules which see both lasers simultaneously, and from neutrals which see neither laser; the latter dark interval records ions created primarily as a result of collisional and field ionization, and is necessary in order to insure

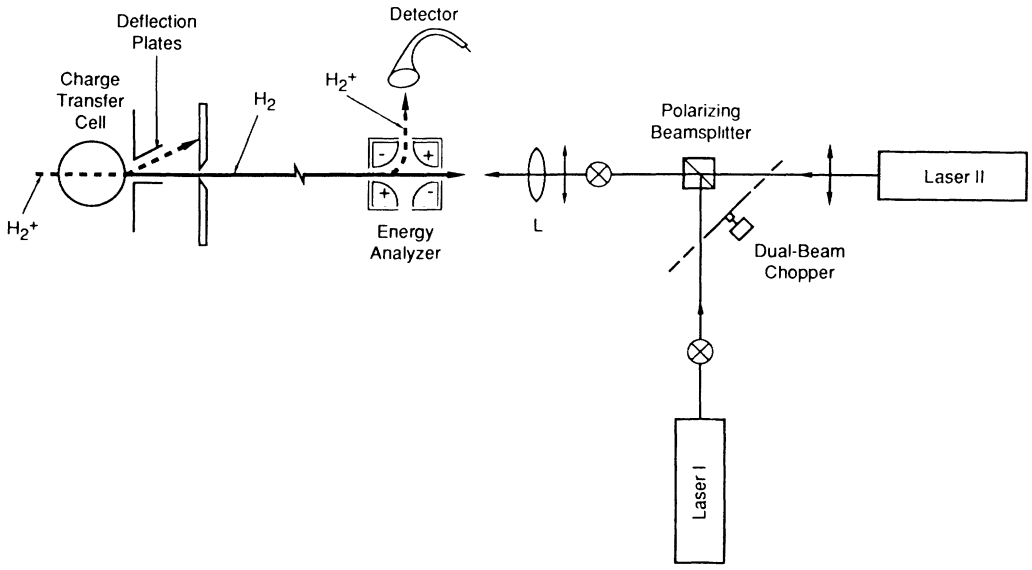


FIG. 2. Experimental arrangement. Depicted here are a portion of the fast-beam apparatus and the optical setup used for double-resonance excitation of the fast $H_2$ beam.

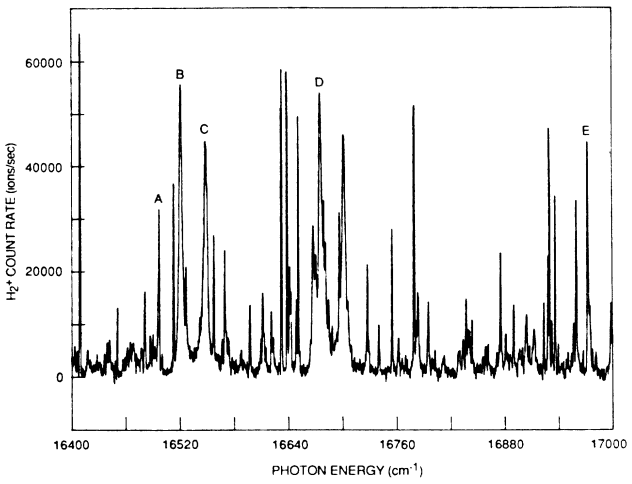


FIG. 3. Typical cw ionization spectrum of $H_2$ $c\,{}^3\Pi_u^-$. Gated scalers and mechanical chopping of the laser are employed to achieve background subtraction.

proper background subtraction. As laser I is frequency tuned, the data-acquisition system thus records two spectra (spectra 1 and 2) corresponding to the ion counts accumulated by the two counters for each laser-I wavelength.

Spectrum 1 will consist of the simple addition of the spectra which would be accumulated by either laser alone: a wavelength-dependent ionization spectrum from laser I, such as that shown in Fig. 3, and the constant ionization induced by the fixed-frequency laser II. In the absence of competition by the two lasers for the same molecules, spectrum 2 would be identical with spectrum 1. However, when laser I and laser II are on at the same time (spectrum 2) and both attempt to excite molecules out of the same lower state, the total ionization rate will be less than the corresponding rate recorded in spectrum

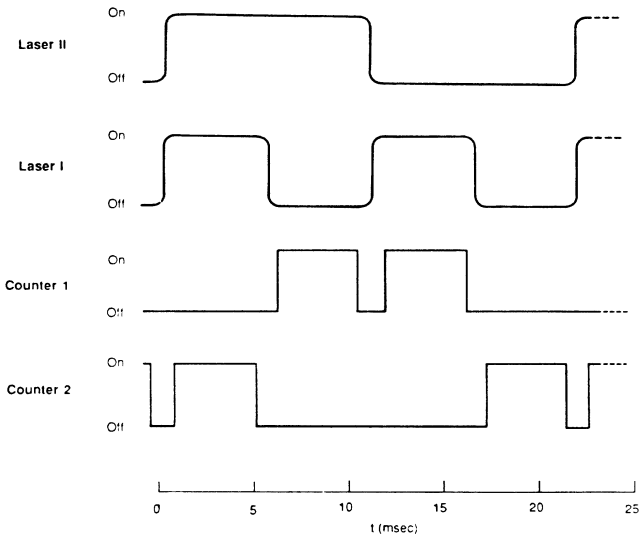


FIG. 4. Duty cycles for the two gated scalers and laser beams. Separate spectra are recorded from the ion counts registered by counters 1 and 2; their difference indicates competition of the two lasers for the same molecules.

1, when the molecular beam is exposed to the two lasers at different times. The difference of spectra 1 and 2 (hereafter the double-resonance or depletion spectrum) should, therefore, display features that indicate any transition (e.g., ionizing or dissociative) whose lower $c$-state level is the same as that for the ionization resonance to which laser II has been tuned. The experimental double-resonance spectra were found to display three types of depletion resonances competing with ionization from the labeled $c$-state level. One class are photoionization transitions; these double resonances were used to clarify the assignment of the photoionization spectra.[13] A second class are transitions to states for which both dissociation and ionization channels are open; these transitions will be discussed in a future paper. A third class are transitions to the rapidly predissociated levels of the $j$ state; in what follows, we specifically discuss these results.

## III. RESULTS AND DISCUSSION

### A. Rovibrational-level assignments

Figures 5(a) and 5(b) show two portions of a typical double-resonance scan. This particular scan was ob-

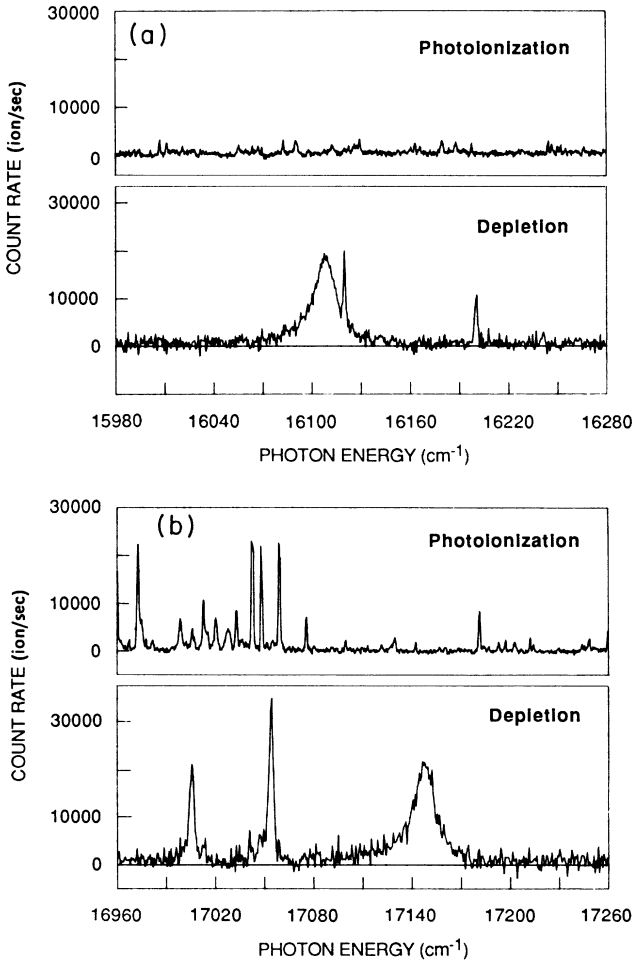


FIG. 5. Associated ionization and double-resonance spectra recorded with laser II tuned to the resonance labeled $A$ in Fig. 3.

tained with laser II tuned to the ionization transition at 16 497.4 $cm^{-1}$ (peak $A$ in Fig. 3). The ionization spectra, obtained with laser I alone, are shown in the top traces of the figure; the corresponding double-resonance (depletion) spectra, obtained by subtracting spectrum 2 from spectrum 1 are shown in the lower traces. In this experiment, laser II produced typically $6\times10^4$ $H_2^+$ ions per second at the labeled photoionization transition; laser I depleted up to 60% of this signal at the strongest double resonance. There are two broad (15 $cm^{-1}$) and four narrow ($\sim$2 $cm^{-1}$) features indicating depletion of the labeled $c$-state level. The broad features in Fig. 5 resemble other depletion resonances observed with laser II tuned to the ionization resonances labeled $B$, $C$, and $D$ (Fig. 3). In no case do these broad resonances have analogous counterparts in the corresponding ionization spectrum.

As will be shown below, these broad resonances represent excitation of the rapidly predissociated $j\,^3\Delta_g$ state, depicted in the potential diagram of Fig. 1. The level diagram in Fig. 6 helps to illustrate the situation; shown here are the observed dissociation transitions from $N''=1$ to $N'=2$. Altogether, nine ionization transitions were used for the current double-resonance experiments; their transition energies are listed in Table I. The ionization transitions used to generate the double-resonance signals in Fig. 5 is also shown in Fig. 6 in order to indicate the general location of the open ionization channels.

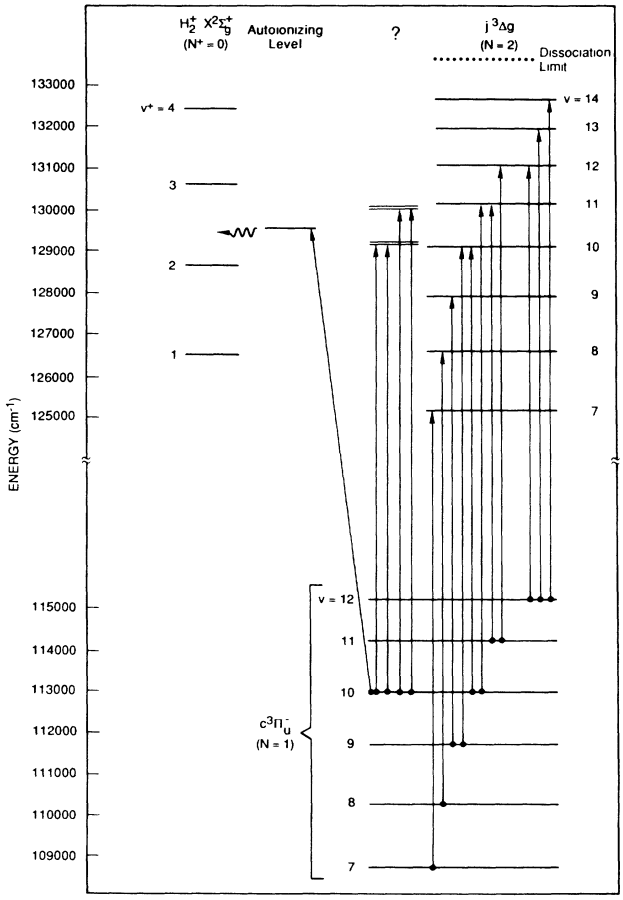


FIG. 6. Energy-level diagram for some of the observed transitions. Dissociation transitions are represented by vertical lines; the inclined line represents the ionization transition corresponding to peak $A$ in Fig. 3. Energy scale referenced to $v=0$ level of the (ground) $X\,^1\Sigma_g^+$ state.

The assignment of the broad dissociation transitions is made possible by accurate Born-Oppenheimer potential curves for the $c$ and $j$ states. Kolos and Rychlewski[14] have calculated the potential-energy curve and rovibrational energies for the $c$ state. Rychlewski[15] has published energies for the $j$ state, but as he has kindly pointed out,[16] the potential curve as listed in his Table I is in error at the internuclear separation $R=1.2$ a.u. This error also affects the vibrational energies listed in his Table IV. Using the corrected[16] energy $V(R=1.2)=-0.584\,371\,73$ a.u. and a numerical eigenvalue-search routine,[17] we have calculated a new set of rovibrational energies for the $j$ state. The reliability of our numerical method was checked by calculating the rovibrational energies of the $c$ state; the resulting values agree with those of Kolos and Rychlewski[14] to within 0.5 $cm^{-1}$. Table II lists the results of our calculations for the $j$ state. Energies are given for the lowest possible rotational levels ($N=2$) of a $\Delta$ ($\Lambda=2$) state, assuming an effective potential energy curve given by the expression

$$V_{\text{eff}}=V+\frac{\hbar}{2\mu R^2}[N(N+1)-\Lambda^2]\ . \tag{1}$$

Rotational constants are also given, having been calculated for the hypothetical rotationless ($N=\Lambda=0$) state.

The assignments for the dissociation transitions are based on analyses such as those discussed here in detail for Fig. 5. The difference in the experimental transition energies of the broad resonances in Fig. 5 is $1042\pm2$ $cm^{-1}$, and must equal the energy spacing of the two rapidly dissociating upper-state levels. This upper-state spacing is consistent with the theoretical spacing of 1041.8 $cm^{-1}$ between the $N'=2$ levels of $v'=10$ and $v'=11$ of the $j\,^3\Delta_g$ state, as predicted by our calculations. The energies of the two broad dissociation transitions in Fig. 5 are within 10 $cm^{-1}$ of the theoretically predicted energy differences between the $v''=10, N''=1$ level of the $c$ state[14] and the corresponding aforementioned upper $j$-state levels. If the two broad transitions are assigned to these rotational levels of the $c$ and $j$ states, they are identified as $R(1)$ transitions from an $N''=1$ level to $N'=2$ levels of the $j$ state. Since the $j$ state is a $\Delta$ state, there is only one rotational transition allowed from any $N''=1$ level; the absence of rotational structure in the double-resonance spectra is consistent with this assignment.

The results shown in Fig. 5 are not by themselves definitive proof for the proposed assignment. However, the other transitions listed in Table I and shown graphically in Fig. 6 share common upper as well as lower-state levels and produce similar agreement with theoretical predictions on the two electronic states involved. When considered in this broader context, no doubt remains concerning the assignment of $c$- and $j$-state levels.

Table III summarizes the comparison between theoretical and experimentally inferred energy spacings for rovi-

TABLE I. Observed transition energies and widths, in $cm^{-1}$. $\Gamma_i$ denotes the autoionization linewidth, $\Gamma_d$ denotes the predissociation linewidth.

| Lower state $c\,^3\Pi_u^-$ | | Ionization transition $E$[a] | $\Gamma_i$ | Upper state $j\,^3\Delta_g$ | | Depletion transition $E$ | $\Gamma_d$ |
|---|---|---|---|---|---|---|---|
| $v''$ | $N''$ | | | $v'$ | $N'$ | | |
| 7 | 1 | 18 172[b] | <1 | 7 | 2 | 16 539±1 | 29±1 |
| 8 | 1 | 17 796[b] | <1 | 8 | 2 | 16 392±1 | 24±1 |
| 9 | 1 | 16 383.5[b] | <1 | 9 | 2 | 16 249±1 | 20±1 |
| | | | | 10 | 2 | 17 403±1 | 15±1 |
| | | | | 10 | 2 | 16 109±1 | 16±1 |
| | | | | 11 | 2 | 17 149±1 | 15±1 |
| 10 | 1 | 16 497.4 (*A*) | <1 | ?[c] | ?[c] | 16 120±1 | 1.7±0.5 |
| | | | | ?[c] | ?[c] | 16 200±1 | 2.2±0.5 |
| | | | | ?[c] | ?[c] | 17 006±1 | 3.5±0.5 |
| | | | | ?[c] | ?[c] | 17 054±1 | 2.9±0.5 |
| 11 | 1 | 16 674.4 (*D*) | 4±1 | 11 | 2 | 15 976±1 | 15±1 |
| | | | | 12 | 2 | 16 894±1 | 15±1 |
| 11 | 3 | 16 549.6 (*C*) | 5±1 | 12 | 3 | 16 813±3 | 20±4 |
| | | | | 12 | 4 | 16 910±3 | 45±5 |
| 11 | 3 | 16 522.7 (*B*) | 4±1 | 12 | 3 | 16 813±3 | 24±4 |
| ? | ? | 16 972.9 (*E*) | <1 | ?[c] | ?[c] | 16 887±1 | 4±1 |
| | | | | 12 | 2 | 15 852±1 | 14±1 |
| 12 | 1 | 15 658[b] | 4±1 | 13 | 2 | 16 642±1 | 11±1 |
| | | | | 14 | 2 | 17 295±1 | 10±1 |

[a] (*A*)–(*E*) denote those lines labeled in Fig. 3.
[b] Ionization resonance outside the spectra region shown in Fig. 3.
[c] Transitions to $n=4$ manifold.

TABLE II. Dissociation energies of lowest rotational levels ($N=\Lambda=2$) and rotational constants of $j\,^3\Delta_g$ state, calculated using corrected (Ref. 16) Rychlewski potential for $H_2$ using a reduced mass value of 0.503 626 5. All values in $cm^{-1}$.

| $v$ | $D_v$ | $B_v$ |
|---|---|---|
| 0 | 21 184.9 | 29.4 |
| 1 | 18 975.5 | 27.8 |
| 2 | 16 892.6 | 26.4 |
| 3 | 14 932.9 | 24.9 |
| 4 | 13 091.9 | 23.5 |
| 5 | 11 367.6 | 22.2 |
| 6 | 9757.3 | 20.8 |
| 7 | 8259.8 | 19.5 |
| 8 | 6874.5 | 18.2 |
| 9 | 5601.9 | 16.8 |
| 10 | 4443.2 | 15.4 |
| 11 | 3401.4 | 14.0 |
| 12 | 2480.6 | 12.5 |
| 13 | 1687.2 | 10.9 |
| 14 | 1030.5 | 9.17 |
| 15 | 522.9 | 7.18 |
| 16 | 181.2 | 4.86 |

brational levels of the $c$ and $j$ states. It is seen that comparison with theory is excellent for the $c$-state spacings; the theoretical $j$-state spacings are consistently larger than the experimental ones, although the agreement is within 5 $cm^{-1}$.

The $j \leftarrow c$ transition energies listed in Table I also constitute a direct measurement of the $j\,^3\Delta_g$ level energies relative to the lower $c$-state levels. These experimental values are listed in Table IV and compared with the theoretical calculations; the experimental $c$-state energies, inferred from the transition-energy differences, are listed for completeness. The zero of energy is taken to be the $v''=9, N''=1$ level of the $c\,^3\Pi_g$ state. The theoretical energies of the $j$ state are calculated based on the Born-Oppenheimer difference of 15 241.3 $cm^{-1}$ between the $n=2$ and 3 limits of the $H + H(nl)$ system, i.e., based on the infinite-mass Rydberg. This infinite-mass Rydberg approximation is one contribution to the adiabatic corrections to the Born-Oppenheimer potential curves; it amounts to a correction of $+8$ $cm^{-1}$ in the difference between the $c$- and $j$-state dissociation limits.

The final column of Table IV notes the discrepancy between the theoretical and experimental level energies. The agreement of the experimental $c$-state energies with

TABLE III. Comparison of theoretical and experimentally inferred energy spacings. Δ indicates the difference between theory and experiment.

| | States | Energy spacings ($cm^{-1}$) Theory[a,b] | Experiment |
|---|---|---|---|
| $c\,^3\Pi_u^-$ | $(v=9,N=1)$ to $(v=10,N=1)$ | 1296.6 | 1294±2 |
| | $(v=10,N=1)$ to $(v=11,N=1)$ | 1172.0 | 1173±2 |
| | $(v=11,N=1)$ to $(v=11,N=3)$ | 153.8 | 152±2[c] |
| | $(v=11,N=1)$ to $(v=12,N=1)$ | 1043.0 | 1042±2 |
| $j\,^3\Delta_g$ | $(v=9,N=2)$ to $(v=10,N=2)$ | 1158.6 | 1154±2 |
| | $(v=10,N=2)$ to $(v=11,N=2)$ | 1041.8 | 1040±2 |
| | $(v=11,N=2)$ to $(v=12,N=2)$ | 920.8 | 918±2 |
| | $(v=12,N=2)$ to $(v=13,N=2)$ | 793.4 | 790±2 |
| | $(v=13,N=2)$ to $(v=14,N=2)$ | 656.8 | 653±2 |
| | $(v=12,N=2)$ to $(v=12,N=3)$ | 74.3 | 72±4 |
| | $(v=12,N=3)$ to $(v=12,N=4)$ | 97.6 | 97±4 |

[a] $c$-state values from Kolos and Rychlewski (Ref. 14).
[b] $j$-state values calculated using corrected potential curve of Rychlewski (Refs. 15 and 16).
[c] Inferred from double-ionization resonance experiments.

theory merely reflects the already noted congruity between the theoretical and experimental rovibrational energy differences recorded in Table III. Similarly, the trend in Δ for the $j$-state levels mirrors the cumulative differences between the theoretical and experimental energy spacings for that state.

While we consider the agreement between theoretical and experimental $j$-state energies to be very good, the discrepancies are nevertheless greater than the experimental uncertainties. The origin of this residual difference is uncertain. The effect of the adiabatic corrections is unknown for the triplet states under consideration, but for the analogous states in the $H_2$ singlet manifold, adiabatic corrections are known to decrease the $C$-to-$J$ state band origin by 93 $cm^{-1}$.[14,18] Near the $j$-state dissociation limit, one might expect the effect of these adiabatic corrections to be dominated by the aforementioned reduced-mass correction; this would lower the theoretical $j$-state energies in Table IV by 8 $cm^{-1}$, which actually increases the discrepancy with theory.

The $j$-state levels under consideration here lie in the dissociation continuum of the two remaining $3d$ states, $3d\pi$ ($i\,^3\Pi_g$) and $3d\sigma$ ($g\,^3\Sigma_g^+$); this results in $j$-state level shifts caused by $l$ uncoupling. The effect of $l$ uncoupling in the $3d$ complex is sketched in Sec. III B; suffice it here to note that our calculations indicate that these shifts are also insufficient to explain the discrepancy between theoretical and experimental $c$-to-$j$ state transition energies.

The assignment of the narrow transitions that appear

TABLE IV. Comparison of experimental and theoretical energies. All energies in $cm^{-1}$.

| | State | | Theory[a,b] | Experiment | Δ |
|---|---|---|---|---|---|
| | $v''$ | $N''$ | | | |
| $c\,^3\Pi_u$ | 9 | 1 | 0 | c | c |
| | 10 | 1 | 1296.59 | 1294±2 | 3±2 |
| | 11 | 1 | 2468.54 | 2467±3 | 2±3 |
| | 11 | 3 | 2619.44 | 2619±3 | 0±3 |
| | 12 | 1 | 3511.53 | 3509±3 | 3±3 |
| | $v'$ | $N'$ | | | |
| $j\,^3\Delta_g$ | 9 | 2 | 16234.2 | 16249±1 | −14±1 |
| | 10 | 2 | 17392.8 | 17403±2 | −10±2 |
| | 11 | 2 | 18434.6 | 18443±2 | −8±2 |
| | 11 | 3 | 18517.9 | 18524±4 | −6±4 |
| | 12 | 2 | 19355.5 | 19361±3 | −5±3 |
| | 12 | 3 | 19429.8 | 19432±5 | −2±5 |
| | 12 | 4 | 19527.4 | 19529±5 | −1±5 |
| | 13 | 2 | 20148.8 | 20151±4 | −2±5 |
| | 14 | 2 | 20805.6 | 20804±4 | 2±4 |

[a] $c$-state values from Kolos and Rychlewski (Ref. 14).
[b] $j$-state values calculated using corrected potential curve of Rychlewski (Refs. 15 and 16).
[c] Experimental values derived assuming this level to agree exactly with theory.

in Fig. 5 and similar spectra is more complex. The upper-state levels accessed in the narrow transitions in Fig. 5 are depicted in the column designated "?" of Fig. 6. We attribute these to $Q(1)$ and $R(1)$ transitions to the $n=4$ $^3\Pi_g$ state. For the vibrational levels involved here, the $n=4$ manifold is strongly perturbed by the lowest doubly excited $^3\Pi_g$ and $^3\Sigma_g$ states, and we have observed both ionization and dissociation for the discrete levels in the $n=4$ states. A detailed discussion of this system will be part of a future publication.

We wish to point out that the assignments for the $c$ $^3\Pi_u$-state levels, obtained here from assignment of the predissociated $j$-state levels, is consistent with the independent assignment of the ionization transitions.[13]

### B. The effects of configuration interaction

The appearance of broad dissociation resonances such as those seen in Fig. 5 results from the configuration interaction between bound and continuum states.[19] Specifically, the bound $j$-state levels and the continuum of the $i$ $^3\Pi_g$ state (see Fig. 1) perturb each other via rotational coupling; the pertinent matrix element is given by the $J_{\pm}L_{\mp}$ interaction terms arising from the nuclear kinetic energy Hamiltonian. If the transition moment to the continuum state is negligible, excitation of the predissociated $j$-state resonances should result in symmetric Lorentzian profiles with a width given by Fermi's golden rule:[20]

$$\Gamma(v,N)=2\pi \mid V_E \mid ^2\rho(\epsilon) , \tag{2}$$

where

$$V_E=[N(N+1)-2]^{1/2}\langle \phi_\Pi \mid L_- \mid \phi_\Delta \rangle \times \langle \chi_\Pi(N,\epsilon) \mid -\hbar^2/2\mu R^2 \mid \chi_\Delta(N,v) \rangle \tag{3}$$

and $\rho(\epsilon)$ is the $i$-state continuum density of states:[7]

$$\rho(\epsilon)=\left[\frac{2}{h}\right](2\mu/\epsilon)^{1/2} \tag{4}$$

and the coupling matrix element is taken from Ref. 21. In Eqs. (2)–(4) the $\chi$'s are vibrational wave functions and the $\phi$'s are electronic wave functions; $E$ is the energy of the $v,N$ $j$-state level, while $\epsilon$ denotes the kinetic energy of the dissociation fragments. The continuum wave function $\chi_\Pi(N,\epsilon)$ is normalized to have unity modulus asymptotically.

In addition to causing predissociation of the $j$-state levels, the rotational interaction induces a shift in the position of the $j$-state level. This shift is given by Fano[19] as

$$F(E_0)=P\int dE' \mid V_{E'} \mid ^2/(E_0-E') . \tag{5}$$

Where $P$ denotes the principal part for the integral and $V_{E'}$ the rotational interaction matrix element [Eq. (3)] between the unperturbed discrete $j$-state level of energy $E_0$ and the continuum $i$-state eigenfunction of energy $E'$. For use in Eq. (5), the continuum wave function appearing in the matrix element $\mid V_{E'} \mid$ must be energy-normalized.[19] We have used Eq. (5) to estimate the $l$-uncoupling shift induced by the $i$ state on the $v'=10$ level of the $j$ state. The result is a 2-cm$^{-1}$ increase in the theoretical energy of this $j$-state level; this small shift is unable to account for the discrepancy between theory and experiment noted in Table IV and discussed in the previous section.

If the "discrete" $j$- and the $i$-state continuum have comparable transition moments from the $c$ state, an asymmetric excitation ("Fano-Beutler") profile will result. Examples of this are common in ionization studies but relatively rare in dissociation studies. The asymmetry arises from an interference of optical transitions to the continuum and bound states, which become inextricably mixed as a result of the configuration interaction. The resonance shape will depend upon the relative strength of the aforementioned transitions, and contains information regarding the relative phases of the wave functions describing the initial $c$-state level, the unperturbed $i$-state continuum, and the bound $j$-state level.

Asymmetric resonances of this type have been observed previously in dissociation.[22,7] In these previous studies, resonances often overlap, due in part to the rovibrational distribution of the lower states involved. The double-resonance technique employed here helps to overcome this difficulty. The asymmetry characteristic of the effects being discussed is evident in Figs. 5 and 7, where we show the profiles of various $R(1)$ transitions. The resonances appear superimposed on a nonzero background value of the double-resonance signal. This indicates transitions to the $i$-state continuum far from the discrete $j$-state level, and must be present whenever configuration interaction causes an asymmetric line shape to appear. It should be noted that in addition to the $N'=2$ continuum of the $i$ $^3\Pi_g$ state, the $N'=1$ continua of the $i$ state and the $g$ $^3\Sigma_g^+$ state, which are free from interaction with the $j$ $^3\Delta_g$ state, contribute to this nonzero background.

Quantitatively, the asymmetry in the excitation profile

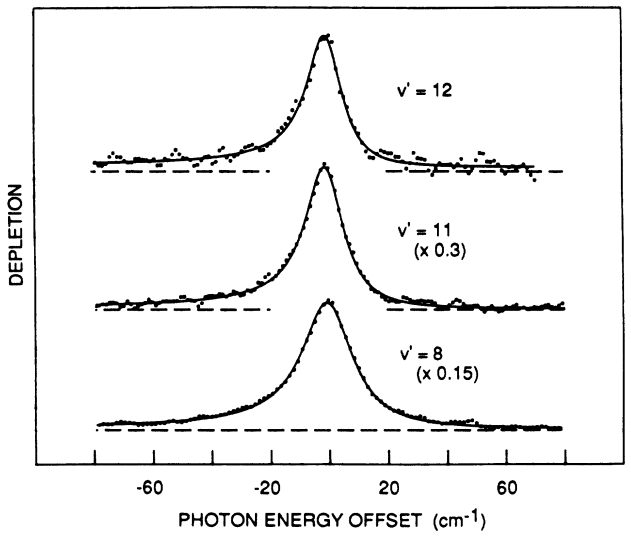


FIG. 7. Photodissociation line profiles for selected $N'=2$ levels of the $j$ $^3\Delta_g$ state, $v'=8,11,12$. Experimental data are shown as points. Solid curve represents best fit of Eq. (3). $q$ parameters obtained from best fit are listed in Table V.

$f(\epsilon)$ is characterized by the dimensionless Fano $q$ parameter which characterizes the generalized line-shape function $f(\epsilon)$:

$$f(\epsilon)=\frac{(q+\epsilon)^2}{1+\epsilon^2} \ . \tag{6}$$

In (6) the reduced energy parameter is

$$\epsilon=\frac{E-E_0'}{\frac{1}{2}\Gamma} \ , \tag{7}$$

where $E_0'$ is the perturbed resonance energy, $E_0+F(E)$, and $\Gamma$ is the configuration-interaction-induced linewidth given by Eq. (2). The asymmetry parameter $q$ depends on the relative transition strength to the discrete and continuum states.[19] Perfectly symmetric resonances will occur only in the limits where the optical transition couples the initial state exclusively to the continuum ("window resonances") or exclusively to the perturbed discrete state (symmetric Lorentzian), and are characterized by $q$ values of 0 to $\infty$, respectively. For the system under consideration here, transition moments tend to favor excitation of the discrete state, resulting in profiles that are only weakly asymmetric.

The experimental dissociation profiles shown in Fig. 7 were fit to a line shape describing the superposition of a Fano profile onto a constant background:

$$AF(\epsilon)+B \ , \tag{8}$$

where the constant $B$ represents excitation to continuum states that are not coupled to the $j$ state. These fits are included in Fig. 7 as full lines. The best-fit $q$ values for the Fano-profile terms are listed in Table V. The line shape represented by Eq. (8) falls to a minimum when the Fano profile equals zero; this occurs at a photon-energy offset of $\frac{1}{2}\Gamma q$ cm$^{-1}$. For all profiles shown, this minimum occurs at photon energies greater than those included in the figure. Since the ratio of peak height to background for a Fano profile is approximately equal to $q^2$, the minima would be difficult to discern visually given the $q$ values listed in Table V. In addition, the noise levels in this experiment would not permit an accurate measurement of the continuum strength. In cases such as these, the asymmetry parameter $q$ therefore serves as a useful alternative measure for the strength of excitation of the continuum.

The final column of Table I lists the $\Gamma$ parameters resulting from a best fit to Eq. (8) for each of our experimental profiles. The uncertainty limits are statistical limits. For a given vibrational level, Eq. (3) shows that the predissociation widths are expected to increase with the rotational quantum number $N$ in close proportion to $N(N+1)$. Table I shows that the $j$-state resonances for $v'=12$ have measured widths which display this predicted trend for the rotational levels $N'=2$, 3, and 4.

We also see from Table I that the observed widths of the $N'=2$ levels decrease with increasing values of $v$. This dependence arises essentially from the fact that the $\langle\,|R^{-2}|\,\rangle$ matrix element appearing in Eq. (3) decreases monotonically with increasing $v$. With the $i$-state potential of Kolos and Rychlewski[14] and the corrected Rychlewski $j$-state potential, we have generated the appropriate vibrational wave functions and used Eqs. (2)–(4) to calculate the expected theoretical $i\leftarrow j$ predissociation widths. These results are listed in Table VI along with the experimental widths from Table I from all observed $N'=2$ levels of the $j$ state. The theoretical results reproduce the trend in $\Gamma$ with $v$ rather well, and the magnitudes of the theoretical widths are within 30% of the experimental ones.

TABLE V. Best-fit Fano $q$ parameters for resonances displayed in Fig. 7.

| Lower level $c\,^3\Pi_u^-$ | Upper level $j\,^3\Delta_g$ | $q$ |
|---|---|---|
| $v=8, N=1$ | $v=8, N=2$ | $-16\pm3$ |
| $v=10, N=1$ | $v=11, N=2$ | $-13\pm2$ |
| $v=12, N=1$ | $v=12, N=2$ | $-11\pm3$ |

TABLE VI. Theoretical and experimental $j$-state dissociation widths for all observed $N'=2$ levels. $R$ represents the ratio $\Gamma_{\text{theory}}/\Gamma_{\text{expt}}$.

| $v$ | $\Gamma_{\text{theory}}$ | $\Gamma_{\text{expt}}$ | $R$ |
|---|---|---|---|
| 7 | 18 | 29±1 | 0.6 |
| 8 | 16 | 24±1 | 0.7 |
| 9 | 14 | 20±1 | 0.7 |
| 10 | 13 | 15±1 | 0.8 |
| 11 | 11 | 15±1 | 0.7 |
| 12 | 10 | 14±1 | 0.7 |
| 13 | 8 | 11±1 | 0.7 |
| 14 | 7 | 10±1 | 0.7 |

## IV. CONCLUSIONS

We have studied dissociative levels of the $j\,^3\Delta_g$ state of molecular hydrogen through the use of an optical-optical double-resonance technique. Using one laser to label rovibrational levels in the metastable $c\,^3\Pi_u^-$ state by exciting a photoionization transition, we have observed transitions to the dissociative $j$-state levels via their depletion of the labeled $c$-state level. We have identified transitions from high-$v$ levels of the $c$ state, previously observed at lower resolution in photofragmentation studies, to high-$v$ levels of the $j$ state heretofore unobserved. Rovibrational energy spacings within either electronic state are in good agreement with the calculations of Kolos and Rychlewski[14] for the $c\,^3\Pi_u$ state, and our calculations for the $j\,^3\Delta$ state using the corrected form of Rychlewski's potential. The $j\leftarrow c$ transition energies are all within 20 cm$^{-1}$ of the theoretical ones.

The dissociation resonances observed in this experiment reveal weakly asymmetric Beutler-Fano profiles, characteristic of the coupling between and simultaneous

excitation to the bound levels of the $j\,^3\Delta_g$ state and the continuum of the $i\,^3\Pi_g$ state. The observed widths of these resonances are within 30% of those predicted by theory. Studies identical to those described herein have been initiated in the isotopic species HD; these results should serve to complement and further elucidate those reported here for $H_2$.

## ACKNOWLEDGMENTS

This research was supported by the National Science Foundation under Grant No. NSF PHY-8706332, the U. S. Air Force Office of Scientific Research under Contract No. F49620-87-K-0002, as well as a NATO travel grant.

[1]W. Lichten, T. Wik, and T. A. Miller, J. Chem. Phys. **71**, 2441 (1979).
[2]E. E. Eyler and F. M. Pipkin, Phys. Rev. Lett. **47**, 1270 (1981).
[3]E. E. Eyler and F. M. Pipkin, Phys. Rev. A **27**, 2462 (1983).
[4]H. Helm, D. P. de Bruijn, and J. Los, Phys. Rev. Lett. **53**, 1642 (1984).
[5]R. D. Knight and L. Wang, Phys. Rev. Lett. **55**, 1572 (1985).
[6]R. Kachru and H. Helm, Phys. Rev. Lett. **55**, 1575 (1985).
[7]D. P. de Bruijn and H. Helm, Phys. Rev. A **34**, 3855 (1986).
[8]N. Bjerre and H. Helm, Chem. Phys. Lett. **134**, 361 (1987).
[9]E. E. Eyler, R. C. Short, and F. M. Pipkin, Phys. Rev. A **56**, 2602 (1987).
[10]W. Lichten, Phys. Rev. **120**, 848 (1960).
[11]H. Helm and P. C. Cosby, J. Chem. Phys. **86**, 6813 (1987).
[12]H. Helm, in *Invited Papers of the Fourteenth International Conference on the Physics of Electronic and Atomic Collisions, Palo Alto, 1985,* edited by D. C. Lorents, W. E. Meyerhof, and J. R. Peterson (North-Holland, Amsterdam, 1986).
[13]N. Bjerre, S. Keiding, L. Lembo, and H. Helm, Phys. Rev. Lett. **60**, 2465 (1988).
[14]W. Kolos and J. Rychlewski, J. Mol. Spectrosc. **66**, 428 (1977).
[15]J. Rychlewski, J. Mol. Spectrosc. **104**, 253 (1984).
[16]J. Rychlewski (private communication).
[17]J. LeRoy, University of Waterloo, Chemical Physical Research Report No. CP-110, 1979 (unpublished).
[18]P. Quadrelli and K. Dressler, J. Mol. Spectrosc. **86**, 316 (1981).
[19]U. Fano, Phys. Rev. **124**, 1866 (1961).
[20]L. Schiff, *Quantum Mechanics* (McGraw-Hill, New York, 1968).
[21]M. Mizushima, *The Theory of Rotating Diatomic Molecules* (Wiley, New York, 1975), p. 143.
[22]M. Glass-Moujean, J. Breton, and P. M. Guyon, Chem. Phys. Lett. **63**, 591 (1979).